Drying Technology: An International Journal
Publication details, including instructions for authors and subscription information:
http://www.tandfonline.com/loi/ldrt20

Numerical Analysis of Natural Convection in Porous Media Subjected to Electromagnetic Energy Using Local Thermal Nonequilibrium (LTNE) Models

Phadungsak Rattanadecho [a] & Waraporn Klinbun [b]

[a] Department of Mechanical Engineering, Thammasat University (Rangsit Campus), Klong Luang, Pathumthani, Thailand

[b] Rattanakosin College for Sustainable Energy and Environment, Phutthamonthon, Nakhon Pathom, Thailand

Version of record first published: 20 Nov 2012.

To cite this article: Phadungsak Rattanadecho & Waraporn Klinbun (2012): Numerical Analysis of Natural Convection in Porous Media Subjected to Electromagnetic Energy Using Local Thermal Nonequilibrium (LTNE) Models, Drying Technology: An International Journal, 30:16, 1896-1905

To link to this article: http://dx.doi.org/10.1080/07373937.2012.718304

Drying Technology, 30: 1896–1905, 2012

ISSN: 0737-3937 print/1532-2300 online
DOI: 10.1080/07373937.2012.718304

Taylor & Francis
Taylor & Francis Group

Numerical Analysis of Natural Convection in Porous Media Subjected to Electromagnetic Energy Using Local Thermal Nonequilibrium (LTNE) Models

Phadungsak Rattanadecho[1] and Waraporn Klinbun[2]

[1]*Department of Mechanical Engineering, Thammasat University (Rangsit Campus), Klong Luang, Pathumthani, Thailand*

[2]*Rattanakosin College for Sustainable Energy and Environment, Phutthamonthon, Nakhon Pathom, Thailand*

The present work numerically investigates the natural convection of fluid in saturated porous media under an electromagnetic field. The porous medium consists of water and spherical solid particles. The Brinkman–Forchheimer extended Darcy model for the momentum equation is employed, and two energy equations are solved with local thermal nonequilibrium (LTNE) models. The study aims at a comprehensive analysis of the influence of material properties, microwave power levels, and operating frequencies on the transport processes in porous media. The results show that all effects have significant consequences on the flow field and heat transfer in porous media. These findings can explain the phenomena taking place inside saturated porous media in electromagnetic wave drying processes using LTNE and local thermal equilibrium (LTE) models.

Keywords Brinkman–Forchheimer extended Darcy model; Electromagnetic field; Local thermal nonequilibrium; Natural convection; Saturated porous medium

INTRODUCTION

Natural convection in porous media with a uniform heat source has been studied by many researchers.[1,2,4,10,14–18] Furthermore, natural convection under an electromagnetic field has been examined by many investigators.[7,9,13,21,22,27] The use of an electromagnetic field as a heat source is widely implemented in industrial processes such as heating, drying, melting, and pasteurizing. Recently, excellent reviews of the drying process in porous materials using electromagnetic energy were presented by Turner and Ilic,[29] Perre and Turner,[30] Ratanadecho et al.,[31,32] and Nattawut and Rattanadecho.[33]

Salagnac et al.[22] presented a numerical model of the hygrothermal behavior of a rectangular-shaped porous material during combined drying. The temperature, moisture content, and pressure fields were shown in detail. A comparison between the simulated results and experimental data on cellular concrete showed the relevance of this model for the study of combined drying. Cha-um et al.[7] experimentally studied the heating of dielectric materials by microwave with a rectangular waveguide. This work investigated the effects of microwave power level, type of sample, dimension, and placement inside the guide. The results showed that the placement of the sample inside the waveguide had a greater effect on the temperature and power absorbed within the material than the other parameters.

However, almost all previous research has been aimed at the local thermal equilibrium (LTE) on the natural convection in porous medium. The assumption of LTE does not apply when the entrance of a packed column where hot gas flows at a high speed is analyzed.[12] Numerous results have shown the failure of the LTE assumption; see Amiri and Vafai,[3] Quintard,[20] Klinbun et al.[28] Thus, the study of natural convection in porous media under an electromagnetic field based on two energy equations has not been clarified. The results may have several engineering applications in the near future.

In the present work a numerical investigation of natural convection in a saturated porous medium under an electromagnetic field is presented. The porous medium was composed of water and spherical solid particles. The Brinkman–Forchheimer extended Darcy model for the momentum equation was employed and two energy equations were solved with a local thermal nonequilibrium (LTNE) model. The study aims at a comprehensive analysis of the influence of material properties, microwave power levels, and operating frequencies on the transport processes in porous media. The thermal and dielectric properties can be found in Table 1.

MODEL EQUATIONS

Figure 1 shows a schematic diagram of the problem. The container was filled with a saturated porous medium. The porous medium consisted of water and spherical solid

Correspondence: Phadungsak Rattanadecho, Department of Mechanical Engineering, Thammasat University (Rangsit Campus), 99 moo 18 Sukhumvit Road, Klong Luang, Pathumthani, 12120, Thailand; E-mail: ratphadu@engr.tu.ac.th

TABLE 1
Properties used in computations

Properties	Air	Water[a]	Glass beads	Alumina	Lead
ε_r	1.0	$f(T)$	5.1	10.8	6.9
$\tan\delta$	0.0	$f(T)$	0.01	0.0145	0.0139
μ_r	1.0	1.0	1.0	1.0	1.0
ρ	1.205	1000	2500	3750	7660
C_p	1.007	4.186	0.80	1.046	0.448
k	0.0262	0.610	1.0	26.0	82.0

[a]For water, the relative permittivity and loss tangent were taken from Ratanadecho et al.[21] as follows:

$$\varepsilon'_r(T) = 85.56 - 0.3099T - 2.328\times10^{-3}T^2 + 4.107\times10^{-5}T^3 - 1.728\times10^{-7}T^4;$$
$$\tan\delta(T) = 0.2314 - 6.405\times10^{-3}T + 9.37\times10^{5}T^2 + 7.415\times10^{-7}T^3 + 2.415\times10^{-9}T^4$$

particle (water saturation, $s=1$; diameter of particle, $d_p=1.0$ mm; porosity, $\varphi=0.371$). An upper wall was opened and the other walls were thermally insulated. The sample was subjected to an electromagnetic field in TE_{10} mode in the z-coordinate. The power input varied from 300 to 1,000 W. The volume of the sample was $109.22\times54.61\times50\,\text{mm}^3$ ($x\times y\times z$).

Analysis of Electromagnetic Field

This study is based on the following assumptions:

1. Since the electromagnetic field in the TE_{10} mode has no variation of field in the direction between the broad faces, so the analysis of electromagnetic field inside a rectangular waveguide is applicable to consider over the x–z plane.
2. The absorption of microwave energy inside the cavity (by the container and the air) is neglected.
3. The walls of a rectangular waveguide are perfectly conducting walls.

Maxwell's equations were solved to simulate the distribution of the electromagnetic field inside the waveguide.

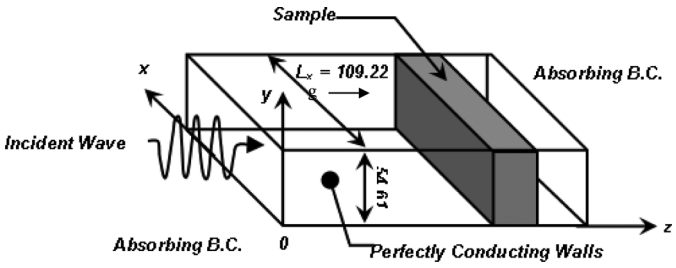

FIG. 1. Schematic diagram of the physical system.

For an electromagnetic wave in TE_{10} mode, the governing equations can be written as:

$$\frac{\partial E_y}{\partial z} = \mu\frac{\partial H_x}{\partial t} \tag{1}$$

$$\frac{\partial E_y}{\partial x} = -\mu\frac{\partial H_z}{\partial t} \tag{2}$$

$$-\left(\frac{\partial H_z}{\partial x} - \frac{\partial H_x}{\partial z}\right) = \sigma E_y + \varepsilon\frac{\partial E_y}{\partial t} \tag{3}$$

where ε is the permittivity or dielectric constant, μ is the magnetic permeability, and σ is the electrical conductivity, which are defined by[21]:

$$\varepsilon = \varepsilon_0\varepsilon_r, \mu = \mu_0\mu_r, \sigma = 2\pi f\varepsilon\tan\delta \tag{4}$$

The dielectric properties or electrical properties of materials can determine the absorption of microwave energy and consequent heating behavior of materials during microwave heating. The dielectric properties are a function of moisture content and temperature, as follows[21]:

$$\varepsilon_r(s,T) = \varepsilon'_r(s,T) - j\varepsilon''_r(s,T) \tag{5}$$

where

$$[\varepsilon'_r(s,T)]^m = \sum_{i=1}^{3}\upsilon_i[\varepsilon'_{ri}(T)]^m = \varphi s[\varepsilon'_{rl}(T)]^m + \varphi(1-s)[\varepsilon'_{ra}]^m + (1-\varphi)[\varepsilon'_{rp}]^m \tag{6}$$

$$[\varepsilon''_r(s,T)]^m = \sum_{i=1}^{3}\upsilon_i[\varepsilon''_{ri}(T)]^m = \varphi s[\varepsilon''_{rl}(T)]^m + \varphi(1-s)[\varepsilon''_{ra}]^m + (1-\varphi)[\varepsilon''_{rp}]^m \tag{7}$$

The parameter m was varied over the range 0–1, as suggested by Wang and Schmugge.[24] For this study, a value of $m=0.33$ was used because this value made the computational dielectric properties close to the measured dielectric properties.

The loss tangent coefficient $\tan\delta$ can be expressed as[21]:

$$\tan\delta = \frac{\varepsilon''_r(s,T)}{\varepsilon'_r(s,T)} \tag{8}$$

The boundary and initial conditions are as follows:

1. A perfect conduction condition was utilized at the surface of the inner walls of the waveguide. Therefore, normal components of the magnetic field and tangential components of the electric field vanish at these walls as follows:

$$H_n = 0, E_t = 0 \tag{9}$$

where subscripts t and n denote the tangential and normal directions, respectively.

2. The first-order absorbing condition by Mur[11] was used at both ends of the waveguide:

$$\frac{\partial E_y}{\partial t} = \pm \upsilon \frac{\partial E_y}{\partial z} \tag{10}$$

where the plus–minus sign represents forward and backward directions and υ denotes the phase velocity of the propagation wave.

3. The input microwave source is simulated by the equations[21]

$$E_y = E_{y\text{in}} \sin\left(\frac{\pi x}{L_x}\right) \sin(2\pi f t) \tag{11}$$

$$H_x = \frac{E_{y\text{in}}}{Z_H} \sin\left(\frac{\pi x}{L_x}\right) \sin(2\pi f t) \tag{12}$$

where f is the frequency of the microwave, L_x is the width of the rectangular waveguide, Z_H is the wave impedance, and $E_{y\text{in}}$ is the input value of the electric field intensity. By applying the Poynting theorem, the input value of the electric field intensity is evaluated by the microwave power input as:

$$E_{y\text{in}} = \sqrt{\frac{4 Z_H P_{\text{in}}}{A}} \tag{13}$$

where P_{in} is the microwave power input and A is the area of the incident plane.

4. The continuity conditions at the interface between different materials are given by:

$$E_t = E_t', H_t = H_t' \tag{14}$$

$$D_n = D_n', B_n = B_n' \tag{15}$$

5. At $t = 0$, all components of E, H are zero.

Analysis of Flow and Temperature Fields

Corresponding to the electromagnetic field, the temperature field and velocity profile can also be assumed to be in a two-dimensional plane (x–z plane). To reduce the complexity of the problem, the following assumptions are applied:

1. The fluid is an incompressible Newtonian fluid.
2. A phase change does not occur.
3. The Boussinesq approximation is applied.
4. The porous medium is isotropic.
5. The effect of the magnetic field on heating is negligible.
6. Thermal dispersion is omitted.

The governing equations for the analysis of flow and heat transfer in this study are as follows:

- Continuity equation:

$$\frac{\partial u}{\partial x} + \frac{\partial w}{\partial z} = 0 \tag{16}$$

- Brinkman–Forchheimer extended Darcy equation (generalized model):

$$\frac{1}{\varphi}\left(\frac{\partial u}{\partial t}\right) + \frac{1}{\varphi^2}\left(u\frac{\partial u}{\partial x} + w\frac{\partial u}{\partial z}\right) = -\frac{1}{\rho_f}\left(\frac{\partial p}{\partial x}\right) + \frac{\nu}{\varphi}\left(\frac{\partial^2 u}{\partial x^2} + \frac{\partial^2 u}{\partial z^2}\right) - \frac{\nu u}{\kappa} - F\left(u^2 + w^2\right)^{1/2} u \tag{17}$$

$$\frac{1}{\varphi}\left(\frac{\partial w}{\partial t}\right) + \frac{1}{\varphi^2}\left(u\frac{\partial w}{\partial x} + w\frac{\partial w}{\partial z}\right) = -\frac{1}{\rho_f}\left(\frac{\partial p}{\partial z}\right) + \frac{\nu}{\varphi}\left(\frac{\partial^2 w}{\partial x^2} + \frac{\partial^2 w}{\partial z^2}\right) - \frac{\nu w}{\kappa} - F\left(u^2 + w^2\right)^{1/2} w + g\beta(T - T_\infty) \tag{18}$$

- The geometric function, F, and permeability, κ, are represented as in Abduk-Rahim and Chamkha[5] and Chamkha et al.[8]:

$$F = \frac{1.75(1-\varphi)}{d_p \varphi^3} \tag{19}$$

$$\kappa = \frac{\varphi^3 d_p^2}{175(1-\varphi)^2} \tag{20}$$

- Fluid-phase energy equation:

$$\varphi\left(\rho C_p\right)_f \frac{\partial T_f}{\partial t} + \left(\rho C_p\right)_f \left(u\frac{\partial T_f}{\partial x} + w\frac{\partial T_f}{\partial z}\right) = k_{feff}\left(\frac{\partial^2 T_f}{\partial x^2} + \frac{\partial^2 T_f}{\partial z^2}\right) + h_{sf} a_{sf}\left(T_s - T_f\right) + \varphi Q \tag{21}$$

- Solid-phase energy equation:

$$(1-\varphi)(\rho C)_s \frac{\partial T_s}{\partial t} = k_{seff}\left(\frac{\partial^2 T_s}{\partial x^2} + \frac{\partial^2 T_s}{\partial z^2}\right) - h_{sf} a_{sf}\left(T_s - T_f\right) + (1-\varphi) Q \tag{22}$$

where Q is the local electromagnetic heat generation term, which is a function of the electric field and is defined as:

$$Q = 2\pi f \varepsilon_0 \varepsilon_r' (\tan\delta) \cdot \left(E_y\right)^2 \tag{23}$$

The porosity is assumed to vary exponentially with a distance of domain.[3,6,19] Based on previous studies, we propose a variation in porosity within three confined walls of the bed: a bottom wall and two lateral walls. The expression that considers the variation in porosity in two directions in the x–z plane is given by

$$\varphi = \varphi_\infty \left[1 + a_1 \left\{ \exp\left(\frac{-a_2 x}{d_p}\right) + \exp\left(-\frac{a_2(W-x)}{d_p}\right) + \exp\left(-\frac{a_2 z}{d_p}\right) \right\}\right] \quad (24)$$

where φ_∞ is the free-stream porosity, which is the porosity far away from the walls; W is the width of the packed bed; and a_1 and a_2 are empirical constants. In this study, $a_1 = 0.98$, $a_2 = 1.00$. These values were suggested by Vafai.[23]

Formulation of the fluid-to-solid heat transfer coefficient, h_{sf}, and the specific surface area of the packed bed, a_{sf}, can be represented as[3]:

$$h_{sf} = k_f \left[2 + 1.1 \mathrm{Pr}^{1/3} \left(\frac{u d_p}{\nu_f}\right)^{0.6}\right] \Big/ d_p. \quad (25)$$

$$a_{sf} = \frac{6(1-\varphi)}{d_p} \quad (26)$$

Because in this work the effects of thermal dispersion are omitted, the thermal conductivity can be defined as:

$$k_{feff} = \varphi k_f \quad (27)$$

$$k_{seff} = (1-\varphi) k_s \quad (28)$$

The boundary and initial conditions are as follows:

1. Upper surface: heat loss via natural convection and the Marangoni flow effect:

$$-k \frac{\partial T}{\partial z} = h_c (T - T_\infty) \quad (29)$$

$$\eta \frac{\partial u}{\partial z} = -\frac{d\xi}{dT} \frac{\partial T}{\partial x} \quad (30)$$

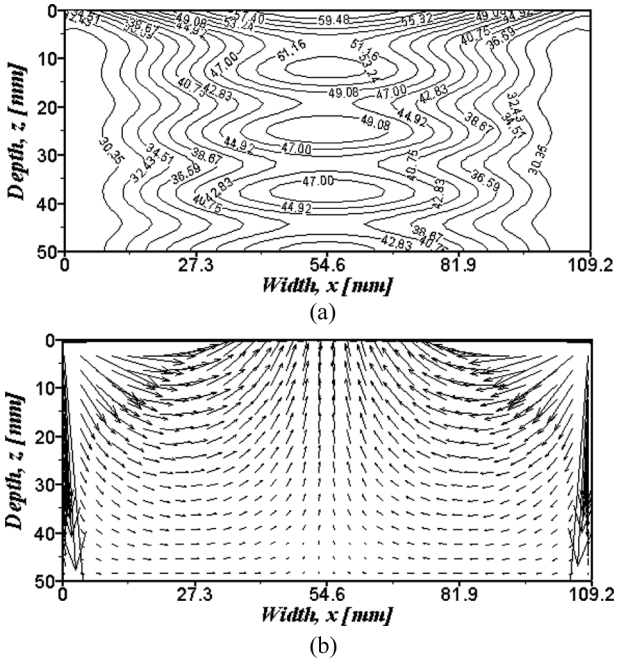

(a)

(b)

FIG. 2. Temperature contour and velocity field for the equilibrium model.

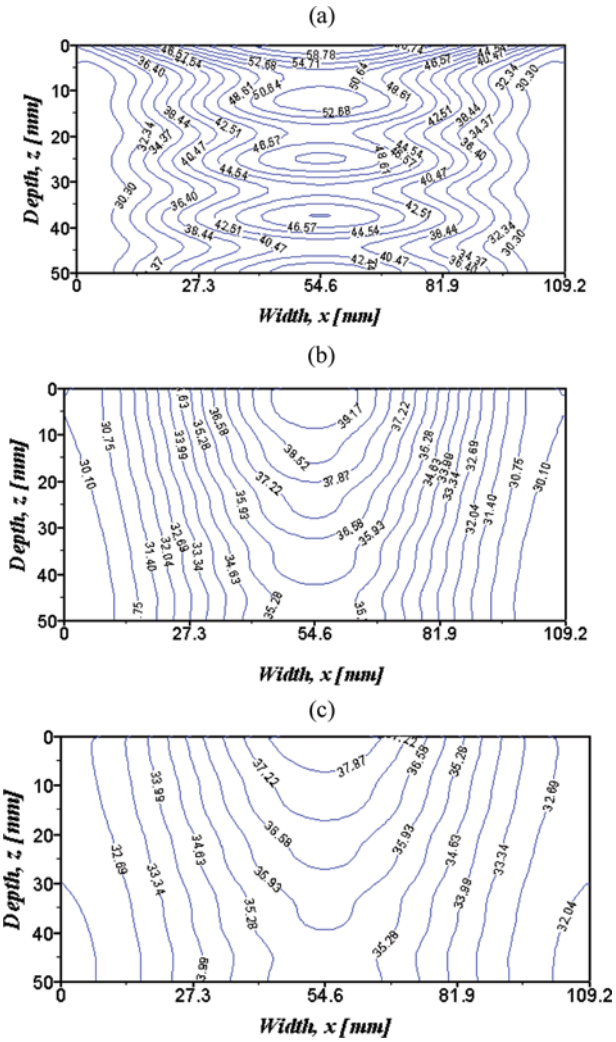

(a)

(b)

(c)

FIG. 3. Temperature contour of the fluid phase for the nonequilibrium model for various types of particles (color figure available online).

where k, h_c are the thermal conductivity and heat transfer coefficient, respectively; η is dynamic viscosity and ξ is surface tension.

2. Other walls of container: thermal insulation and no-slip boundary conditions are applied.

$$\frac{\partial T_f(x,z)}{\partial n} = \frac{\partial T_s(x,z)}{\partial n} = 0 \tag{31}$$

$$\left.\begin{array}{l} u = 0, x = 0, 109.22\text{mm} \\ w = 0, z = 50\text{mm} \end{array}\right\} \tag{32}$$

3. Initial condition ($t = 0$s)

$$T_0 = T_f = T_s = 28^{\circ}\text{C} \tag{33}$$

Numerical Solution Procedures

The description of heat transport and flow pattern, Eqs. (16)–(23), requires specification of temperature (T), velocity components (u, w), and pressure (p). These equations were coupled to Maxwell's equations (Eqs. (1)–(3)) by Eq. (23). This equation represents the heating effect of the microwaves in the packed bed–container domain. The electromagnetic equations were solved using a finite difference time domain method. With this method, the electric field components (E) are stored halfway between the basic nodes and the magnetic field components (H) are stored at the center. Hence, they are calculated at alternating half time steps. The E and H field components are discretized by a central difference method (second-order accurate) in both the spatial and time domains.

Spatial and temporal resolution was selected to ensure stability and accuracy. To ensure stability of the

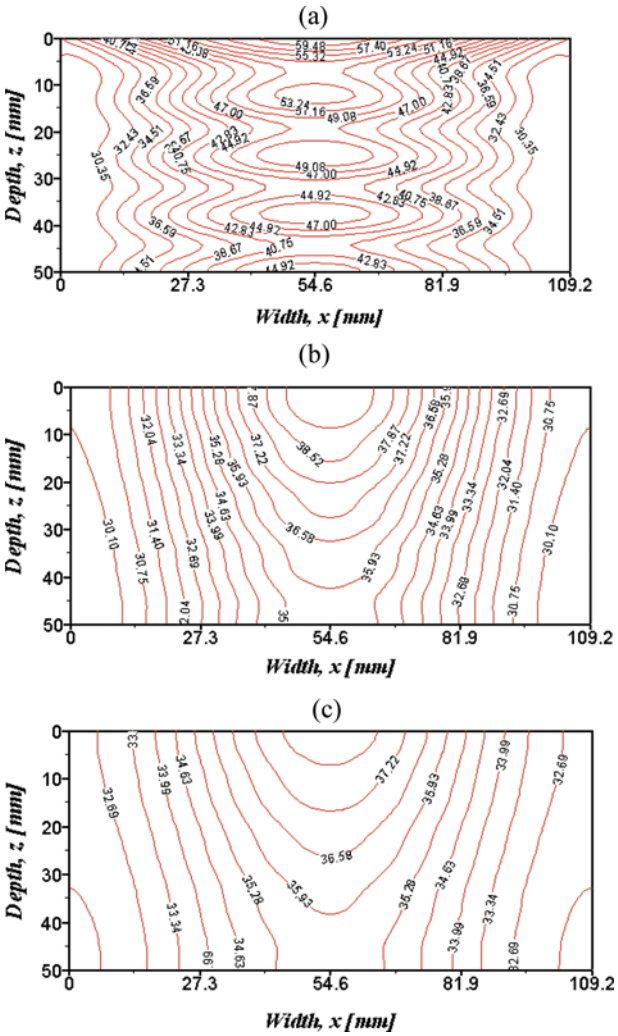

FIG. 4. Temperature contour of the solid phase for the nonequilibrium model for various types of particles (color figure available online).

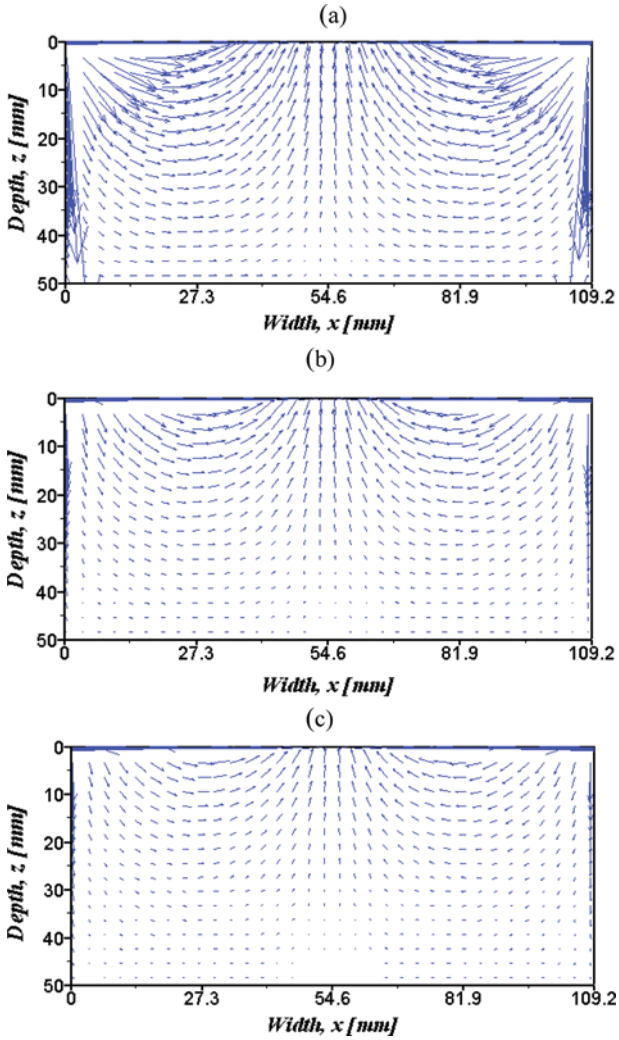

FIG. 5. Velocity field for the nonequilibrium model for various types of particles (color figure available online).

time-stepping algorithm, Δt was chosen to satisfy the Courant stability condition:

$$\Delta t \leq \frac{\sqrt{(\Delta x)^2+(\Delta z)^2}}{\upsilon}. \quad (34)$$

The spatial resolution of each cell was defined as:

$$\Delta x, \Delta z \leq \frac{\lambda_g}{10\sqrt{\varepsilon_r}} \quad (35)$$

Corresponding to Eqs. (34) and (35), the calculation conditions were as follows: $\Delta x = 1.0922$ mm, $\Delta z = 1.0000$ mm, and $\Delta t = 2 \times 10^{-12}$ s.

Equations (16)–(22) were solved numerically using the finite control volume method with the SIMPLE algorithm developed by Patankar.[25] This method has the advantage of flux conservation, and it avoids generation of a parasitic source. The basic strategy of the finite control volume discretization method is to divide the calculated domain into a number of control volumes and then integrate the conservation equations over this control volume over a time interval $[t, t+\Delta t]$. At the boundaries of the calculated domain, the conservation equations are discretized by integrating over half of the control volume and taking into account the boundary conditions. At the corners of the calculated domain, a quarter of the control volume is used. The fully implicit time discretization finite difference scheme is used to arrive at the solution in time. The time step is $\Delta t = 0.01$ s and relative error in the iteration procedures of 10^{-6} was chosen. Details regarding numerical discretization using this method can be found in the literature.[25,26]

RESULTS AND DISCUSSION

In this study, the saturated porous packed bed consisted of water and spherical solid particles, and the properties for computation are shown in Table 1. Three types of particles with a diameter of 1.0 mm and porosity of 0.371 were considered; that is, alumina, glass beads, and lead. The following results show the effects of the type of solid particle, power input level, and operating frequencies on heat transport phenomena in a saturated porous packed bed.

Local Thermal Equilibrium Model

Figure 2 shows the temperature contour and velocity field for the case of fluid-saturated porous medium subjected to an electromagnetic field that is in thermodynamical equilibrium. The physical data are as follows: water–glass beads (WG), $P = 500$ W, $f = 2.45$ GHz, $t = 60$ s. In Fig. 2a, the temperature is high at the middle of the sample due to the highest intensity of the electric field in the TE_{10} mode in the middle region of the waveguide. The temperature was distributed to the wall due to the standing wave that is formulated within packed beds. In Fig. 2b, the flow patterns are characterized by the two symmetrical vortices. The fluid flows as it is driven by the effect of buoyancy. This effect is distributed from the upper corner near the surface

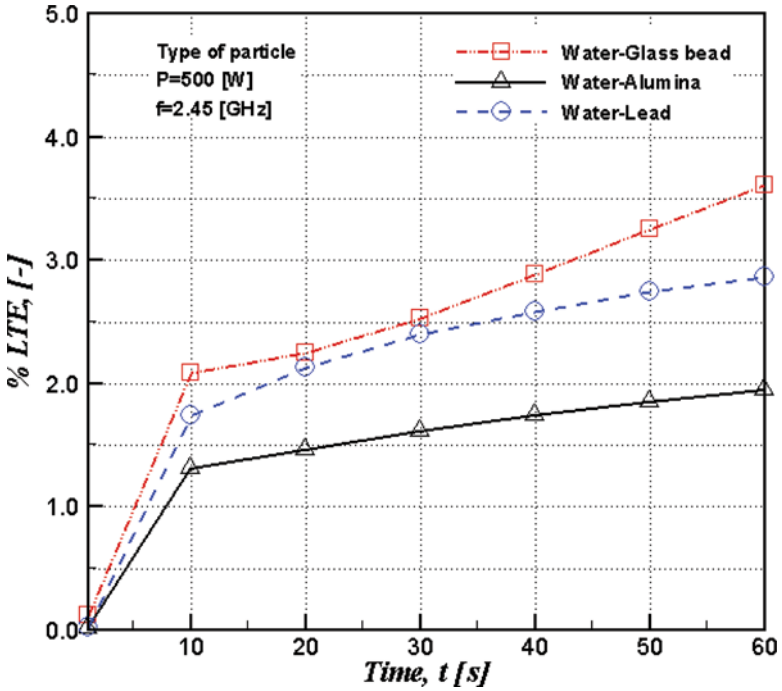

FIG. 6. Percentage difference of temperature distributions of the solid and fluid phases for various types of particles during the operating time (color figure available online).

where the incident wave propagates through. The buoyancy effect is associated with the lateral temperature gradient at locations near the top surface. Heated portions of the fluid become lighter than the rest of fluid and are expanded laterally away from the center to the sides then flow down along the two vertical walls, leading to the clockwise and counterclockwise flow circulation.

Effect of Type of Solid Particles

This section discusses the effect of various types of solid phase (glass bead, alumina, and lead). The fluid phase as water is supposed to consist of a saturated porous packed bed for all three types of solid particles. The volume of the porous packed bed is $109.22 \times 54.61 \times 50\,\text{mm}^3$. The physical conditions are as follows: $P = 500\,\text{W}$, $f = 2.45\,\text{GHz}$, and operating time $(t) = 60\,\text{s}$.

The temperature contours of the fluid phase, solid phase, and velocity field are shown in Figs. 3–5, respectively. The simulations are shown in the x–z plane of a porous packed bed at $t = 60\,\text{s}$. As seen in Figs. 3 and 4, the temperature was highest at the center of the packed bed and was distributed to the wall due to the standing wave formulated within the packed bed. The temperature contour of the fluid phase was similar to the that of the solid phase. Figure 5 shows the flow patterns with a packed bed for various types of particles. Fluid flow fields are displayed in the same direction but the magnitudes of the flows are clearly different. The explanation of the flow behavior is similar to that discussed in the previous section.

Figure 6 shows the percentage of difference of temperature distributions of the solid and fluid phases for various types of solid particles during the operating time. It was found that the percentage difference of temperature of the solid and fluid phases was maximum corresponding to the porous packed bed of water–glass beads. This was due to the lower dielectric properties of the glass beads.

Furthermore, to classify the outcome on qualitative ratings for the LTE assumption, this may be expressed in the following form[3]:

$$\%\text{LTE} = \left|T_{s(i,k)} - T_{f(i.k)}\right| \times 100 \tag{36}$$

The following categories for grading the results were adopted: very good, less than 1%; good, 1–5%; fair, 5–10%; poor 10–15%; and very poor, more than 15%.

As shown in Fig. 6, the maximum value was 3.61%. It is in good level of LTE assumption. Thus, we can use the LTE assumption to analyze the temperature of the porous packed bed in this situation.

Effect of Microwave Power Level

Next, we will consider the effect of the power input level. The power input levels were 300, 500, and 1,000 W, respectively. A porous packed bed of water–glass beads with a volume of $109.22 \times 54.61 \times 50\,\text{mm}^3$ was utilized. A frequency of 2.45 GHz and operating time of 60 s were used.

Figures 7a and 7b show the temperature distributions of the solid and fluid phases at various power input levels, along with the horizontal axis ($z = 10\,\text{mm}$) and vertical axis ($x = 54.61\,\text{mm}$) of a rectangular waveguide, respectively. For water–glass beads, the porous packed bed with $P = 1{,}000\,\text{W}$ corresponded to a higher temperature than that for the porous packed bed with $P = 300\,\text{W}$ for x and z directions. This was due to the high power input, which affected the local electromagnetic heat generation (Q) and thus created the temperature difference.

In Fig. 7a, the temperature was highest at the center of the packed bed because the intensity of the electric field in

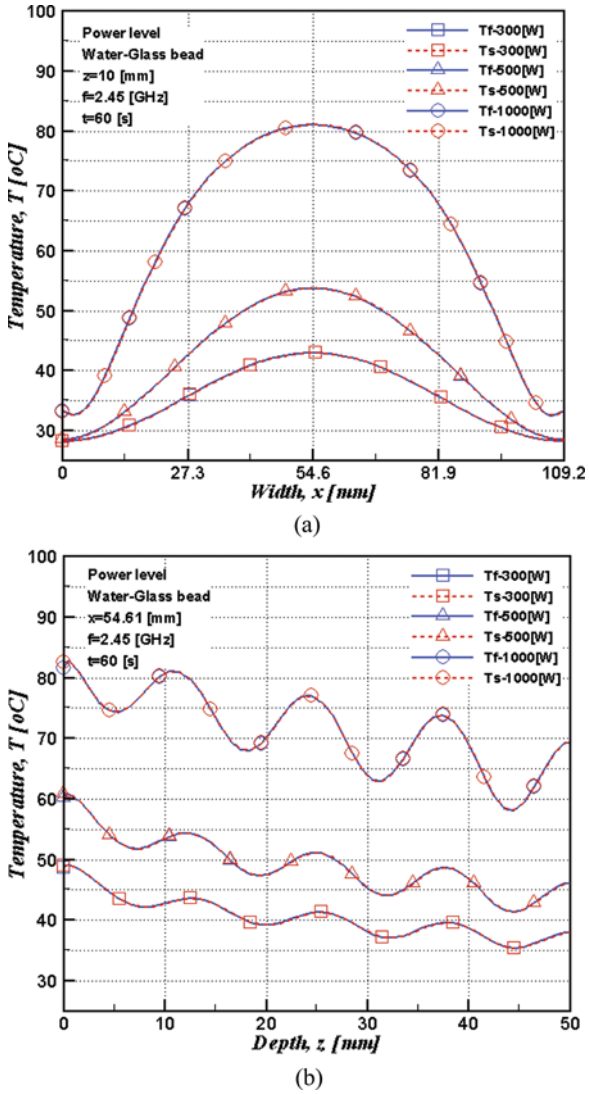

FIG. 7. Temperature distributions of the solid and fluid phases at various power input levels: (a) along the x-axis and (b) along the z-axis (color figure available online).

TE_{10} mode was high around middle of the guide. In Fig. 7b, the highest temperature occurred at the surface of the packed bed and decreased along the depth of the packed bed due to the microwave penetration depth. From Fig. 7, it can be seen that the temperatures of fluid and solid were not very different. The difference is clarified in Fig. 8.

Figure 8 illustrates the percentage of the temperature difference vs. time distributions for various power input levels. The result is similar to Fig. 6. It was observed that the percentage of the temperature difference was much larger for the porous packed bed at $P = 1{,}000$ W, whereas the porous packed bed at $P = 300$ W corresponded to smaller percentage of temperature difference during 60 s. However, in Fig. 8, the maximum value of the difference was 8.01% for the case of a bed packed with water–glass beads with $P = 1{,}000$ W. Thus, from Eq. (36), the LTE assumption was used to analyze the heat transfer for this situation.

Effect of Operating Frequency

Lastly, the effect of operating frequency was studied. The operating frequencies used were 1.50, 2.45, and 5.80 GHz. The volume of the packed bed of water–lead was $109.22 \times 54.61 \times 50\,\text{mm}^3$. The power level was fixed at 500 W and the operating time was 60 s.

Figures 3c, 9a, and 9b show temperature contour of the fluid phase at operating frequencies of 2.45, 1.50, and 5.80 GHz, respectively, and the temperature profiles of the solid phase are shown in Figs. 4c, 10a, and 10b. From Figures 9 and 10, the temperature was greatest at the surface exposed to the incident wave and decayed exponentially along the propagation wave. At the higher frequency (5.80 GHz), the wave had a small penetration depth, so the electric field decayed much faster compared

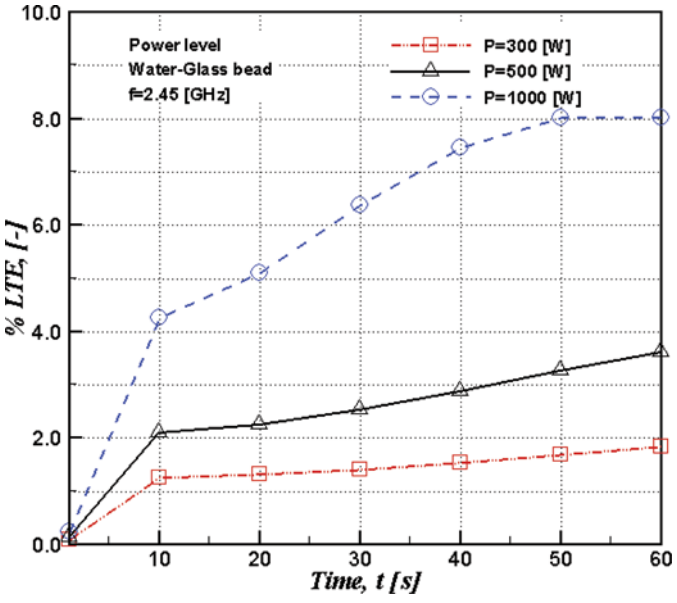

FIG. 8. Percentage difference of temperature distributions of the solid and fluid phases at various power input levels during the operating time (color figure available online).

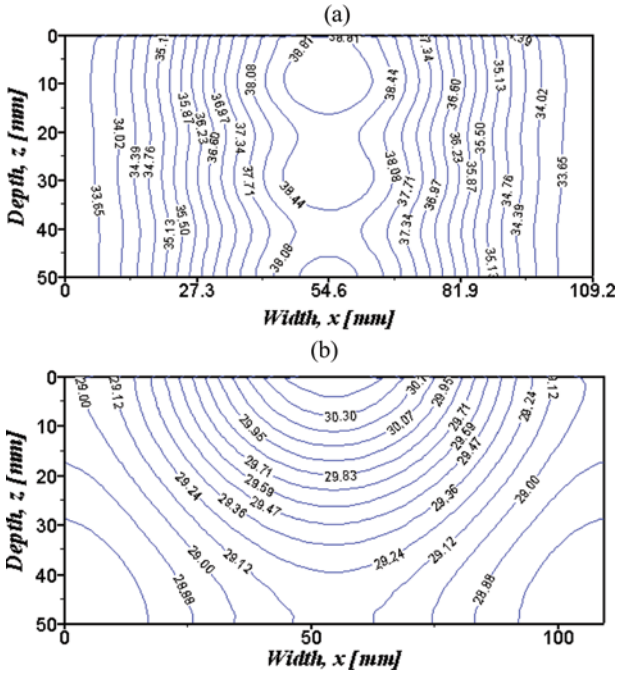

FIG. 9. Temperature contour of the fluid phase for the nonequilibrium model for various operating frequencies (color figure available online).

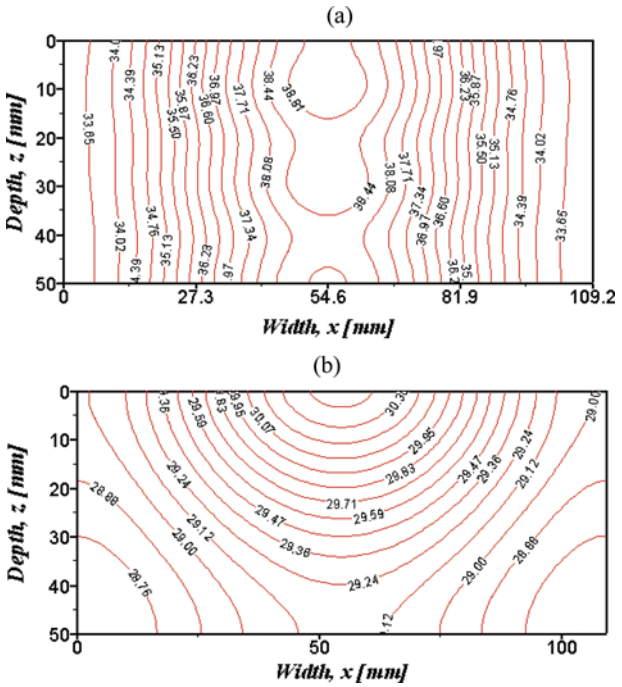

FIG. 10. Temperature contour of the solid phase for the nonequilibrium model for various operating frequencies (color figure available online).

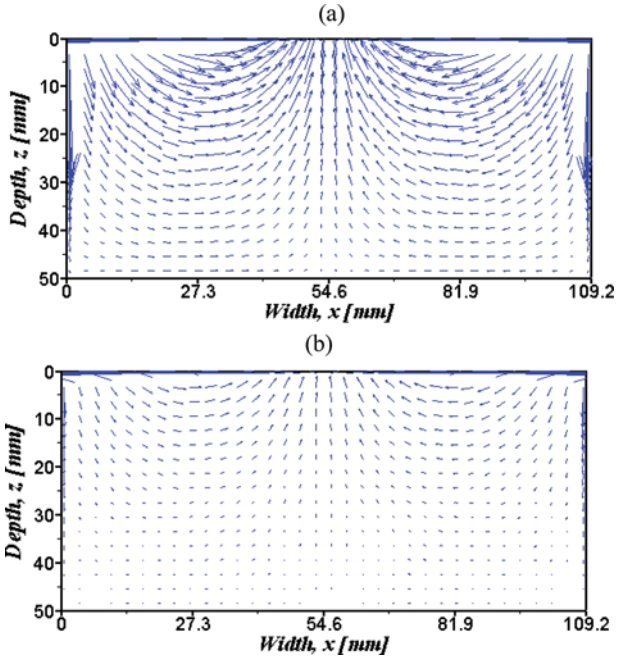

FIG. 11. Velocity field for the nonequilibrium model for various operating frequencies (color figure available online).

other operating frequencies and resulted in a thinner thermally stratified layer (as seen in Figs. 9b and 10b).

The flow patterns within the porous packed bed at operating frequencies of 2.45, 1.50, and 5.80 GHz are shown in Figs. 5c, 11a, and 11b, respectively. The flow fields display in the same direction but are clearly different in flow magnitude. The explanation of fluid flow is similar to that discussed previously.

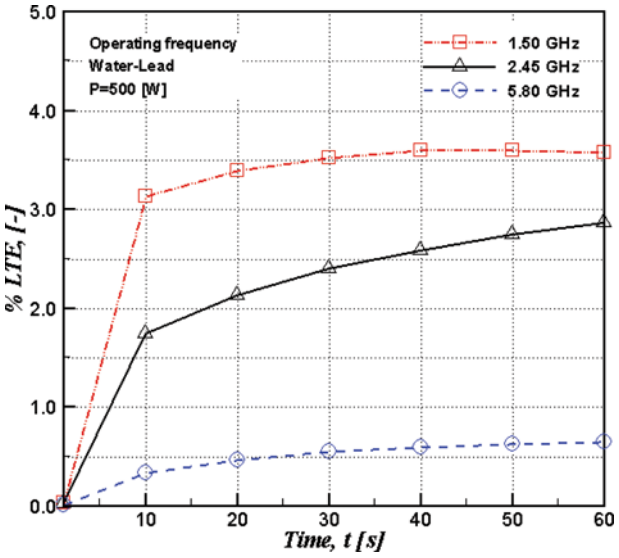

FIG. 12. Percentage difference of temperature distributions of the solid and fluid phases at various operating frequencies during the operating time (color figure available online).

Figure 12 shows the percentage of the temperature difference vs. time distributions for various operating frequencies. It was found that the maximum difference was 3.60% for the case of water–lead with $f = 1.50$ GHz.

CONCLUSIONS

Two energy equations for a fluid-saturated porous media were calculated numerically. The effects of the type of solid particles and power input level on the transport processes in porous media were studied in detail. The major findings from this work are as follows:

1. Material properties, such as type of particle and dielectric properties, significantly affected the percentage of different temperature between two phases.
2. Operating conditions (microwave power and frequency) affected the heat generation in each phase.
3. Finally, all effects on transport processes in a porous packed bed were significant, but the LTE model can be used for analysis in this situation.

These results will aid researchers in understanding the drying of porous media subjected to electromagnetic energy using LTNE and LTE models and can be applied in the industrial field.

NOMENCLATURE

a	Specific surface area of a packed bed (m^{-1})
E	Electric field intensity (Vm^{-1})
f	Frequency (Hz)
H	Magnetic field intensity (Am^{-1})
p	Pressure (Pa)
P	Power (W)
Pr	Prandtl number
Q	Heat generation term (Wm^{-3})
s	Saturation
T	Temperature (°C)
t	Time (s)
$\tan\delta$	Loss tangent
u, w	Velocity component (ms^{-1})

Greek Letters

α	Thermal diffusivity (m^2s^{-1})
β	Coefficient of thermal expansion (K^{-1})
ε	Permittivity (Fm^{-1})
κ	Permeability (m^2)
μ	Magnetic permeability (Hm^{-1})
σ	Electric conductivity (Sm^{-1})
φ	Porosity

Subscripts

a	Air
eff	Effective
f	Fluid
l	Liquid
r	Relative

s	Solid
x, y, z	Coordinates

ACKNOWLEDGMENTS

This work was supported by the Thailand Research Fund and the National Research University Project of the Thailand Office of Higher Education Commission.

REFERENCES

1. Nield, D.A.; Bejan, A. *Convective in Porous Media*; Springer-Verlag: New York, 1999.
2. Vafai, K. *Handbook of Porous Media*; Marcel Dekker: New York, 2004.
3. Amiri, A.; Vafai, K. Analysis of dispersion effects and non-thermal equilibrium, non-Darcian, variable porosity incompressible flow through porous media. *International Journal of Heat and Mass Transfer* **1994**, *37*, 939–954.
4. Al-Amiri, A.M. Analysis of momentum and energy transfer in a lid-driven cavity filled with a porous medium. *International Journal of Heat and Mass Transfer* **2002**, *43*, 3513–3527.
5. Abdul-Rahim, A.K.; Chamkha, A.J. Variable porosity and thermal dispersion effects on coupled heat and mass transfer by natural convection from a surface embedded in a non-metallic porous medium. *International Journal of Numerical Methods for Heat and Fluid Flow* **2001**, *11*, 413–429.
6. Benenati, R.F.; Brosilow, C.B. Void fraction distribution in pack beds. *AIChE Journal* **1962**, *8*, 359–361.
7. Cha-um, W.; Rattanadecho, P.; Pakdee, W. Experimental analysis of microwave heating of dielectric materials using a rectangular wave guide (mode: TE_{10}) (case study: water layer and saturated porous medium). *Experimental Thermal and Fluid Science* **2009**, *33*(3), 472–481.
8. Chamkha, A.J.; Issa, C.; Khanafer, K. Natural convection from an inclined plate embedded in a variable porosity porous medium due to solar radiation. *International Journal of Thermal Sciences* **2002**, *41*, 73–81.
9. Dinčov, D.D.; Parrot, K.A.; Pericleous, K.A. Heat and mass transfer in two-phase porous materials under intensive microwave heating. *Journal of Food Engineering* **2004**, *65*, 403–412.
10. Khanafer, K.M.; Chamkha, A.J. Mixed convection flow in a lid-driven enclosure filled with a fluid-saturated porous medium. *International Journal of Heat and Mass Transfer* **1998**, *42*(13), 2465–2481.
11. Mur, G. Absorbing boundary conditions for the finite difference approximation of the time domain electromagnetic field equations. *IEEE Transactions on Electromagnetic Compatibility* **1981**, *23*, 377–382.
12. Nakayama, A.; Kuwahara, F.; Sugiyama, M.; Xu, G. A two-energy equation model for conduction and convection in porous media. *International Journal of Heat and Mass Transfer* **2001**, *44*, 4375–4379.
13. Ni, H.; Datta, A.K.; Torrance, K.E. Moisture transport in intensive microwave heating of biomaterials: Porous media model. *International Journal of Heat and Mass Transfer* **1999**, *42*, 1501–1512.
14. Nithiarasu, P.; Seetharamu, K.N.; Sundararajan, T. Natural convective heat transfer in a fluid saturated variable porosity medium. *International Journal of Heat and Mass Transfer* **1997**, *40*(16), 3955–3967.
15. Nithiarasu, P.; Seetharamu, K.N.; Sundararajan, T. Numerical investigation of buoyancy driven flow in a fluid saturated non-Darcian porous medium. *International Journal of Heat and Mass Transfer* **1998**, *42*(7), 1205–1215.
16. Oosthizen, P.H.; Patrick, H. *Natural Convection in an Inclined Square Enclosure Partly Filled with a Porous Medium and with a Partially Heated Wall*, HTD 302; American Society of Mechanical Engineers, Heat Transfer Division: New York, 1995, 29–42.
17. Prasad, V.; Kulacki, F.A. Convective heat transfer in a rectangular porous cavity—Effect of aspect ratio on flow structure and heat transfer. *Journal of Heat Transfer* **1994**, *106*, 158–165.
18. Pakdee, W.; Rattanadecho, P. Unsteady effects on natural convective heat transfer through porous media in cavity due to top surface partial convection. *Applied Thermal Engineering* **2006**, *26*(17–18), 2316–2326.
19. Poulikakos, D.; Renken, K. Forced convection in a channel filled with porous medium, including the effects of flow inertia, variable porosity and Brinkman friction. *Journal of Heat Transfer* **1987**, *109*, 880–888.
20. Quintard, M. Modelling local thermal non-equilibrium heat transfers in porous media. In *Proceedings of the Eleventh International Heat Transfer Conference*, Kyongju, Korea, August 23–28, 1998; 369–464.
21. Ratanadecho, P.; Aoki, K.; Akahori, M. Influence of irradiation time, particle sizes, and initial moisture content during microwave drying of multi-layered capillary porous materials. *Journal of Heat Transfer* **2002**, *124*(1), 151–161.
22. Salagnac, P.; Glouannec, P.; Lecharpentier, D. Numerical modeling of heat and mass transfer in porous medium during combined hot air, infrared and microwave drying. *International Journal of Heat and Mass Transfer* **2004**, *47*, 4479–4489.
23. Vafai, K. Convective flow and heat transfer in variable-porosity media. *Journal of Fluid Mechanics* **1984**, *147*, 233–259.
24. Wang, J.; Schmugge, T. An empirical model for the complex dielectric permittivity of soil as a function of water content. *IEEE Transactions on Geoscience and Remote Sensing* **1980**, *18*(4), 288–295.
25. Patankar, S.V. *Numerical Heat Transfer and Fluid Flow*; Hemisphere: New York, 1980.
26. Yee, K.S. Numerical solution of initial boundary value problems involving Maxwell's equation in isotropic media. *IEEE Transactions on Antennas and Propagation* **1996**, *14*, 302–307.
27. Klinbun, W.; Rattanadecho, P. Analysis of microwave induced natural convection in a single mode cavity (influence of sample volume, placement, and microwave power level). *Applied Mathematical Modelling* **2012**, *36*(2), 813–828.
28. Klinbun, W.; Vafai, K.; Rattanadecho, P. Electromagnetic field effects on transport through porous media. *International Journal of Heat and Mass Transfer* **2012**, *55*(1–3), 325–335.
29. Turner, I.W.; Ilic, M. Combined microwave and convective drying of a porous material. *Drying Technology* **1991**, *9*(5), 1209–1269.
30. Perre, P.; Turner, I.W. A3D version of TransPore: A comprehensive heat and mass transfer computational model for simulating the drying of porous media. *International Journal of Heat and Mass Transfer* **1999**, *42*(24), 4501–4521.
31. Ratanadecho, P.; Aoki, K.; Akahori, M. Experimental and numerical study of microwave drying in unsaturated porous material. *International Communications in Heat and Mass Transfer* **2001**, *28*(5), 605–616.
32. Rattanadecho, P.; Pakdee, W.; Stakulcharoen, J. Analysis of multiphase flow and heat transfer: Pressure buildup in an unsaturated porous slab exposed to hot gas. *Drying Technology* **2008**, *26*(1), 39–53.
33. Nattawut, S.; Rattanadecho, P. Analysis of heat–mass transport and pressure buildup induced inside unsaturated porous media subjected to microwave energy using a single (TE10) mode cavity. *Drying Technology* **2011**, *29*(9), 1010–1024.